Post-perovskite CaIrO₃: A $j = 1/2$ quasi-one-dimensional antiferromagnet

Nikolay A. Bogdanov,[1] Vamshi M. Katukuri,[1] Hermann Stoll,[2] Jeroen van den Brink,[1] and Liviu Hozoi[1]

[1]*Institute for Theoretical Solid State Physics, IFW Dresden, Helmholtzstrasse 20, 01069 Dresden, Germany*
[2]*Institute for Theoretical Chemistry, Universität Stuttgart, Pfaffenwaldring 55, 70550 Stuttgart, Germany*

The $5d^5$ iridate CaIrO₃ is isostructural with the post-perovskite phase of MgSiO₃, recently shown to occur under extreme pressure in the lower Earth's mantle. It therefore serves as an analog of post-perovskite MgSiO₃ for a wide variety of measurements at ambient conditions or achievable with conventional multianvile pressure modules. By multireference configuration-interaction calculations we here provide essential information on the chemical bonding and magnetic interactions in CaIrO₃. We predict a large antiferromagnetic superexchange of 120 meV along the c axis, the same size with the interactions in the cuprate superconductors, and ferromagnetic couplings smaller by an order of magnitude along a. CaIrO₃ can thus be regarded as a $j = 1/2$ quasi-one-dimensional antiferromagnet. While this qualitatively agrees with the stripy magnetic structure proposed by resonant x-ray diffraction, the detailed microscopic picture emerging from our study, in particular, the highly uneven admixture of t_{2g} components, provides a clear prediction for resonant inelastic x-ray scattering experiments.

Iridium oxide compounds are at the heart of intensive experimental and theoretical investigations in solid state physics. The few different structural varieties displaying Ir ions in octahedral coordination and tetravalent $5d^5$ valence states, in particular, have recently become a fertile ground for studies of new physics driven by the interplay between strong spin-orbit interactions and electron correlations.[1] The spin-orbit couplings (SOCs) are sufficiently large to split the Ir t_{2g}^5 manifold into well separated $j = 3/2$ and $j = 1/2$ states. The former are fully occupied while the latter are only half filled. It appears that the widths of the $j = 1/2$ bands, $w \sim Nt$, where t is an effective Ir-Ir hopping integral and N is the coordination number, are comparable to the strength of the on-site Coulomb repulsion U. For smaller coordination numbers, such as $N = 3$ in the layered honeycomb systems Li₂IrO₃ and Na₂IrO₃ and $N = 4$ for square-lattice Sr₂IrO₄ and Ba₂IrO₄ and the post-perovskite CaIrO₃, the undoped compounds are insulating at all temperatures and a $j = 1/2$ Mott-Hubbard type picture seems to be appropriate.[1–3] For larger coordination numbers like $N = 6$ in the pyrochlore structure, the t_{2g}^5 Ir oxides are metallic at high T's and display transitions to antiferromagnetic (AF) insulating states on cooling.[4] Here, a Slater-type picture in which the gap opening is intimately related to the onset of AF order might be more appropriate, as proposed for example for Os oxide perovskite systems with $N = 6$.[5] Nevertheless, also more exotic ground states such as a Mott topological insulator[6] or a Weyl semimetal[7] have been proposed for the pyrochlore iridates.

Besides the SOCs and Coulomb interactions, one important additional energy scale is the magnitude of the splittings within the Ir t_{2g} shell. Such splittings may arise from distortions of the O octahedron around the Ir site and also from the anisotropy of the farther surroundings. In this respect, highly anisotropic systems such as the post-perovskite CaIrO₃ provide an ideal playground for new insights into the interplay between SOCs and lattice distortions. In the layered post-perovskite structure, IrO₆ octahedra in the ac layers share corners along the crystallographic c axis, see Fig. 1, and have common edges along a.[8] The Ir-O bonds along the corner-sharing chains are

substantially shorter than for the edge-sharing links, 1.94 vs 2.07 Å, which suggests a stabilization of the xy-like orbital with respect to the xz and yz terms. Additionally, small splittings between the xz and yz components may in principle arise due to the a-b crystal anisotropy.

The precise nature of the relativistic $5d^5$ ground-state wave function obviously depends on the size of the Ir t_{2g} splittings. Further, the on-site $5d^5$ electron configuration and the kind of Ir-O-Ir path along a given direction determine the sign and magnitude of the magnetic exchange couplings. *Ab initio* calculations where all these effects and interactions are treated on equal footing are therefore highly desirable. For this, we focus on the post-perovskite phase of CaIrO₃, which has received significant attention from geologists in recent years because the same crystalline structure is adopted by MgSiO₃ in the lower Earth's mantle.[9,10] In contrast to MgSiO₃, the post-perovskite phase of CaIrO₃ can be synthesized even at ambient pressure. Since measurements are less complicated in ambient conditions, CaIrO₃ has been used extensively as an analog of MgSiO₃ post-perovskite for structural, mechanical, and transport studies.[11–14] To unveil the valence electronic structure of CaIrO₃ we here carry out *ab initio* wave-function quantum chemical calculations. With no SOCs, splittings as large as 0.8 eV are found for the t_{2g} levels of CaIrO₃. The $5d^5$ relativistic ground-state wave function therefore displays a highly uneven admixture of xy, xz, and yz character, which contradicts the interpretation of recent resonant x-ray diffraction (RXD) experiments.[15] For the corner-sharing octahedra, the quantum chemical calculations further predict large AF superexchange couplings[16] of 120 meV, about the same size as the magnetic interactions in the parent compounds of the high-T_c cuprate superconductors. The lowest d-d excited states are two doublets at approximately 0.7 and 1.4 eV, originating from the $j = 3/2$ quartet in an ideal cubic environment. This is the largest splitting reported so far for the $j = 3/2$ quartet in d^5 systems and singles out CaIrO₃ as a unique material in which both the SOC and the noncubic crystal field splittings are of the order of 0.5 eV or larger.
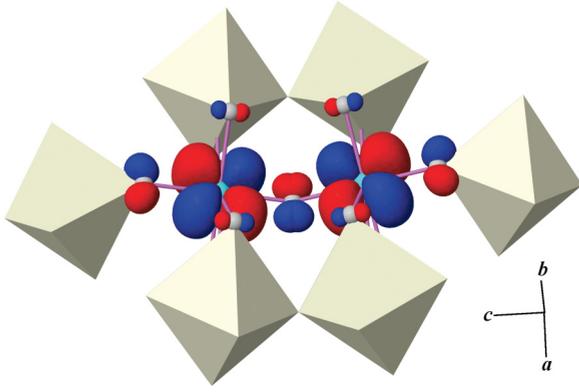
FIG. 1. (Color online) Local coordination and the main, π-type $5d_{xz}$-$2p_x$-$5d_{xz}$ AF superexchange path for corner-sharing IrO_6 octahedra along the c axis in $CaIrO_3$; see text. Nearest-neighbor O ions around the two Ir sites in the center of the figure are shown as small light-grey spheres. Ca ions above and below the IrO_3 layer are not displayed. The O $2p$ tails of the active Ir d_{xz} orbitals are overlapping at the bridging O site.

To investigate the local Ir d-level splittings, multi-configuration self-consistent-field (MCSCF) and multiref-erence configuration-interaction (MRCI) calculations[17] are performed on embedded clusters made of one reference IrO_6 octahedron, ten adjacent Ca sites, and four nearest-neighbor (NN) IrO_6 octahedra. That a realistic representation of ions at NN polyhedra guarantees highly accurate results for the d-level electronic structure at the central site was earlier pointed out for correlated $3d^1$, $3d^2$, and $3d^9$ oxide compounds.[18–20] The farther solid-state environment is modeled as a one-electron effective potential which in an ionic picture reproduces the Madelung field in the cluster region. All calculations are performed with the MOLPRO quantum chemical software.[21] We employed energy-consistent relativistic pseudopotentials for Ir[22] and Ca[23] and Gaussian-type valence basis functions[22–25] (for details, see Supplementary Material[26]). For the ground-state calculations, the orbitals within each finite cluster are variationally optimized at the MCSCF level. All Ir t_{2g} functions are included in the active orbital space. Excitations within the Ir t_{2g} shell are afterwards computed just for the central IrO_6 octahedron while the occupation of the NN Ir valence shells is held frozen as in the MCSCF ground-state configuration. Spin-orbit interactions are further accounted for as described in Ref. 27. The subsequent MRCI treatment includes all single and double excitations from the O $2p$ orbitals at the central octahedron and the Ir $5d$ functions. To partition the O $2p$ valence orbitals into two different groups, i.e., at sites of the central octahedron and at NN octahedra, we employ the orbital localization module available with MOLPRO. Crystallographic data as reported by Rodi and Babel[8] are used.

With no SOCs, we find Ir $d_{xy} - d_{yz}$ and $d_{xy} - d_{xz}$ splittings of 0.63 and 0.76 eV by MCSCF calculations and slightly larger values of 0.68 and 0.83 eV at the MRCI level, with the xy level being the lowest (see the first lines in Table I). The $j = 1/2$ ground-state wave function therefore has dominant xz character, as much as 75% by MRCI calculations with SOC (MRCI + SOC). The four components of the $j = 3/2$ quartet are split into groups of two by 0.6–0.7 eV (lower lines of

TABLE I. Ir t_{2g} splittings and relative energies of the spin-orbit t_{2g}^5 states in $CaIrO_3$. MCSCF and MRCI results are given with and without SOCs for five-plaquette clusters; see text.

t_{2g}^5 splittings (eV)	MCSCF	MRCI
$d_{xy} - d_{yz}$	0.63	0.68
$d_{xy} - d_{xz}$	0.76	0.83
$|j = 1/2, m_j = \pm 1/2\rangle$	0.00–0.12	0.00–0.16
$|j = 3/2, m_j = \pm 3/2\rangle$	0.62–0.70	0.66–0.76
$|j = 3/2, m_j = \pm 1/2\rangle$	1.25–1.27	1.36–1.39

Table I). The lower two $j = 3/2$ terms have 72% yz character, the highest $j = 3/2$ components have 90% xy character.

When SOCs are not accounted for, the coupling to spin moments at NN Ir sites gives rise for each particular orbital occupation to one sextet, four quartet, and five doublet states. All those configuration state functions enter the spin-orbit calculations. Thirty-two different spin-orbit states are therefore generated for each j configuration at the central Ir site and this causes a finite energy spread in Table I. A simpler and more transparent picture can be obtained by replacing the four $Ir^{4+} d^5$ NN's by closed-shell $Pt^{4+} d^6$ ions. In that case, the MRCI excitation energies for the $j = 3/2$ states at the central Ir site are 0.67 and 1.38 eV. An instructive computational experiment which we can further make is to replace the distorted post-perovskite structure by a hypothetical cubic perovskite lattice in which the Ir-O bond length is the average of the three different bond lengths in post-perovskite $CaIrO_3$, i.e., 2.03 Å. This allows one to directly extract the SOC λ for the Ir^{4+} $5d^5$ ion because the splitting between the spin-orbit $j = 1/2$ doublet and the four-fold degenerate $j = 3/2$ state is $3\lambda/2$ in cubic symmetry.[28] The doublet-quartet splitting comes out as 0.70 eV by MRCI + SOC calculations for the idealized cubic perovskite structure. This yields a spin-orbit coupling constant $\lambda = 0.47$, in agreement with values of 0.39–0.49 eV earlier extracted for Ir^{4+} impurities from electron spin resonance measurements.[29]

The results of our *ab initio* calculations, i.e., the unusually large t_{2g} splittings and the highly uneven admixture of xz, yz, and xy character for the spin-orbit t_{2g}^5 states, are in sharp contrast to the interpretation of recent RXD experiments on $CaIrO_3$.[15] In particular, the authors of Ref. 15 conclude from the RXD data that the deviations from an isotropic xz-yz-xy picture are marginal, as also found for instance in the layered square-lattice material Sr_2IrO_4.[1] While for Sr_2IrO_4 we also obtain[30] rather small t_{2g} splittings of about 0.1 eV, comparable weights of the xz, yz, and xy components in the $j = 1/2$ ground-state wave function, and NN superexchange interactions in good agreement with resonant inelastic x-ray scattering (RIXS) data, for the post-perovskite $CaIrO_3$ the quantum chemical results point in a different direction. These conflicting findings urgently call for Ir L-edge RIXS measurements on $CaIrO_3$. The RIXS experiments have recently emerged as a most reliable technique for exploring the charge, spin, and orbital degrees of freedom of correlated electrons in solids.[31,32]

The presence of both corner-sharing and edge-sharing octahedra and the large splittings within the t_{2g} shell have important implications on the nature and the magnitude of the magnetic interactions. To determine the latter, we designed

TABLE II. NN effective magnetic couplings in CaIrO$_3$; see text. Positive values denote AF exchange.

J (meV)	MCSCF	MRCI	MRCI + SOC
J_c	91.2	163.4	121.0
J_a	-2.3	4.2	-7.3

eight-octahedra clusters including two active Ir^{4+} d^5 sites. The six 5d NNs were modeled as closed-shell Pt^{4+} d^6 ions. All possible occupations were allowed within the set of t_{2g} orbitals at the two active Ir sites in the MCSCF calculations, which gives rise to nine singlet and nine triplet states with no SOC. The MCSCF wave functions were expressed in terms of orbitals optimized for an average of those singlet and triplet states. All eighteen singlet and triplet states entered the spin-orbit calculations, both at the MCSCF and MRCI levels. In MRCI, single and double excitations from the Ir t_{2g} orbitals and the 2p orbitals of the bridging ligand were included. Such a computational scheme provides J values in very good agreement with RIXS measurements in the layered iridate Sr$_2$IrO$_4$.[30]

Remarkably, with no SOCs, the NN AF exchange constant J_c for octahedra sharing corners along the c axis is as large as 91.2 meV by MCSCF calculations and 163.4 meV by MRCI; see Table II. The t_{2g} hole orbitals are here the xz components, as discussed above. Although the IrO$_6$ octahedra are tilted somewhat due to rotations about the a axis, see Fig. 1, this does not affect much the π-type 5d_{xz}-2p_x-5d_{xz} overlap and superexchange[16] interactions. An AF J of 163.4 meV is even larger than the values for σ-type superexchange paths in two-dimensional $S = 1/2$ 3d Cu oxide superconductors[33] and points to the role of the larger spatial extent of 5d functions in iridates. With SOCs accounted for, the effective AF coupling J_c is reduced to 121.0 meV (last column in Table II). The spin-orbit ground-state wave function now acquires sizable yz character and, since the tilting of the IrO$_6$ octahedra does affect the out-of-plane 5d_{yz}-2p_y-5d_{yz} superexchange path, the effective magnetic coupling between the $j = 1/2$ sites is smaller.

For edge-sharing octahedra along the a axis, we find a weak NN ferromagnetic (FM) coupling $J_a \approx -7.3$ meV in the spin-orbit MRCI calculations. The three components of the $j_{tot} = 1$ triplet state in the two-site problem display small splittings of ≈ 1 meV (see Supplementary Material[26]), which shows that anisotropic non-Heisenberg terms[34] should also be considered when mapping the *ab initio* data onto an effective spin Hamiltonian. In estimating the Heisenberg coupling constant
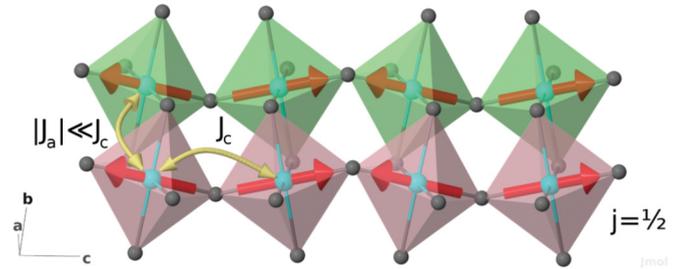

FIG. 2. (Color online) Sketch of the NN magnetic interactions in CaIrO$_3$.

J_a we neglected such terms and used an average of the energies of the $j_{tot} = 1$ triplet components, $J \approx \tilde{E}(j_{tot} = 1) - E(j_{tot} = 0)$. The *ab initio* results, i.e., strong AF interactions along c and weak FM couplings along a (see Fig. 2), are in full agreement with the observed striped AF magnetic ordering.[15] The MRCI + SOC J values thus provide a firm quantitative basis for understanding the magnetic properties of this material.

We have employed, in summary, a set of many-body quantum chemical calculations to unravel the 5d electronic structure of the post-perovskite iridate CaIrO$_3$. While electronic structure calculations have been earlier performed within the local density approximation to density functional theory and the role of electron correlation effects has been pointed out,[35] we here make clear quantitative predictions for the Ir t_{2g} splittings, character of the entangled spin-orbit wave function, and magnitude of the NN superexchange interactions. Our results single out CaIrO$_3$ as a 5d^5 system in which lattice distortions and spin-orbit couplings compete on the same energy scale to give rise to highly anisotropic electronic structure and magnetic correlations. In particular, the present *ab initio* investigation yields a different picture than previously derived on the basis of resonant x-ray diffraction experiments for the relativistic ground-state wave function. The large t_{2g} splittings that we have found from the calculations give rise to dominant xz hole character and remarkably strong AF interactions along the c axis. Further, the large AF couplings along c and weak FM exchange along a characterize CaIrO$_3$ as a $j = 1/2$ quasi-one-dimensional antiferromagnet.

[1] B. J. Kim, H. Ohsumi, T. Komesu, S. Sakai, T. Morita, H. Takagi, and T. Arima, Science **323**, 1329 (2009).

[2] Y. Singh, S. Manni, J. Reuther, T. Berlijn, R. Thomale, W. Ku, S. Trebst, and P. Gegenwart, Phys. Rev. Lett. **108**, 127203 (2012).

[3] K. Ohgushi, H. Gotou, T. Yagi, Y. Kiuchi, F. Sakai, and Y. Ueda, Phys. Rev. B **74**, 241104 (2006).

[4] K. Matsuhira, M. Wakeshima, Y. Hinatsu, and S. Takagi, J. Phys. Soc. Jpn. **80**, 094701 (2011).

[5] S. Calder, V. O. Garlea, D. F. McMorrow, M. D. Lumsden, M. B. Stone, J. C. Lang, J. W. Kim, J. A. Schlueter, Y. G. Shi, K. Yamaura, Y. S. Sun, Y. Tsujimoto, and A. D. Christianson, Phys. Rev. Lett. **108**, 257209 (2012).

[6]D. Pesin and L. Balents, Nat. Phys. **6**, 376 (2010).

[7]X. Wan, A. M. Turner, A. Vishwanath, and S. Y. Savrasov, Phys. Rev. B **83**, 205101 (2011).

[8]F. Rodi and D. Babel, Z. Anorg. Allg. Chem. **336**, 17 (1965).

[9]M. Murakami, K. Hirose, K. Kawamura, N. Sata, and Y. Ohishi, Science **304**, 855 (2004).

[10]A. R. Oganov and S. Ono, Nature (London) **430**, 445 (2004).

[11]N. Miyajima, K. Ohgushi, M. Ichihara, and T. Yagi, Geophys. Res. Lett. **33**, L12302 (2006).

[12]D. C. Martin, K. W. Chapman, P. J. Chupas, V. Parakapenka, P. L. Lee, S. D. Shastri, and J. B. Parise, Am. Mineral. **92**, 1048 (2007).

[13]T. Ballaran, R. Tronnes, and D. Frost, Am. Mineral. **92**, 1760 (2007).

[14]S. A. Hunt, D. R. Davies, A. M. Walker, R. J. McCormack, A. S. Wills, D. P. Dobson, and L. Li, Earth Planet. Sci. Lett. **319–320**, 96 (2012).

[15]K. Ohgushi, J. Yamaura, H. Ohsumi, K. Sugimoto, S. Takeshita, A. Tokuda, H. Takagi, M. Takata, and T. Arima, arXiv:1108.4523.

[16]P. W. Anderson, Phys. Rev. **115**, 2 (1959).

[17]T. Helgaker, P. Jørgensen, and J. Olsen, *Molecular Electronic-Structure Theory* (Wiley, Chichester, 2000).

[18]L. Hozoi, L. Siurakshina, P. Fulde, and J. van den Brink, Sci. Rep. **1**, 65 (2011).

[19]N. A. Bogdanov, J. van den Brink, and L. Hozoi, Phys. Rev. B **84**, 235146 (2011).

[20]L. Hozoi and M. S. Laad, Phys. Rev. Lett. **99**, 256404 (2007).

[21]H.-J. Werner, P. J. Knowles, G. Knizia, F. R. Manby, M. Schütz *et al.* [see http://www.molpro.net].

[22]D. Figgen, K. A. Peterson, M. Dolg, and H. Stoll, J. Chem. Phys. **130**, 164108 (2009).

[23]P. Fuentealba, L. von Szentpaly, H. Preuss, and H. Stoll, J. Phys. B **18**, 1287 (1985).

[24]T. H. J. Dunning, J. Chem. Phys. **90**, 1007 (1989).

[25]K. Pierloot, B. Dumez, P.-O. Widmark, and B. O. Roos, Theor. Chim. Acta **90**, 87 (1995).

[26]See Supplemental Material at http://link.aps.org/supplemental/10.1103/PhysRevB.85.235147 for computational details.

[27]A. Berning, M. Schweizer, H.-J. Werner, P. J. Knowles, and P. Palmieri, Mol. Phys. **98**, 1823 (2000).

[28]A. Abragam and B. Bleaney, *Electron Paramagnetic Resonance of Transition Ions* (Clarendon, Oxford, 1970).

[29]B. Andlauer, J. Schneider, and W. Tolksdorf, Phys. Status Solidi B **73**, 533 (1976).

[30]V. M. Katukuri, H. Stoll, J. van den Brink, and L. Hozoi, Phys. Rev. B **85**, 220402 (2012).

[31]L. J. P. Ament, M. van Veenendaal, T. P. Devereaux, J. P. Hill, and J. van den Brink, Rev. Mod. Phys. **83**, 705 (2011).

[32]J. Schlappa, K. Wohlfeld, K. J. Zhou, M. Mourigal, M. W. Haverkort, V. N. Strocov, L. Hozoi, C. Monney, S. Nishimoto, S. Singh, A. Revcolevschi, J.-S. Caux, L. Patthey, H. M. Ronnow, J. van den Brink, and T. Schmitt, Nature (London) **485**, 82 (2012).

[33]D. Muñoz, F. Illas, and I. de P. R. Moreira, Phys. Rev. Lett. **84**, 1579 (2000).

[34]J. Chaloupka, G. Jackeli, and G. Khaliullin, Phys. Rev. Lett. **105**, 027204 (2010).

[35]A. Subedi, Phys. Rev. B **85**, 020408 (2012).